Direct Numerical Simulation and Transition: 2-D Flows

Helen L. Reed
Texas A&M University
Aerospace Engineering, 602B H.R. Bright Building, 3141 TAMU
College Station, Texas 77843-3141 USA

helen.reed@tamu.edu

1.0 INTRODUCTION

Direct numerical simulations (DNS) are playing an increasingly important role in the investigation of transition; this trend will continue as considerable progress is made in the development of new, extremely powerful computers and numerical algorithms. In such simulations, the full Navier-Stokes equations are solved directly by employing numerical methods, such as finite-difference, finite-element, finite volume, or spectral methods. There are two approaches: 1) simulations in which the disturbances are computed as part of the simulation, and 2) simulations in which transition is estimated based on mean-flow quantities or the location is user specified.

Complementary reviews include that of Kleiser & Zang (1991) and the AGARD lecture on spatial simulations (Reed 1994). Transition is a spatially evolving process and the spatial DNS approach is widely applicable since it avoids many of the restrictions that usually have to be imposed in other models and is the closest to mimicking experiments. For example, very few restrictions with respect to the form or amplitude of the disturbances have to be imposed, because no linearizations or special assumptions concerning the disturbances have to be made. Furthermore, this approach allows the realistic treatment of space-amplifying and -evolving disturbances as observed in laboratory experiments. The temporal simulation, by contrast, uses periodic boundary conditions in the chordwise direction (identical inflow and outflow conditions) and follows the time evolution of a disturbance as it convects through the flow; upstream influence is limited by this assumption. Moreover, in temporal simulations, the basic state is assumed to be strictly parallel, that is, invariant with respect to the chordwise coordinate. All of these restrictions noted are especially suspect when considering complex geometries, 3-D boundary layers, receptivity, control, and the breakdown to turbulence.

The basic idea of the spatial simulation is to disturb an established basic flow by forced, time-dependent perturbations. Then the reaction of this flow, that is, the temporal and spatial development of the perturbations, is determined by the numerical solution of the complete Navier-Stokes equations.

Challenges associated with this method which preclude it from being used routinely for design include:

- A large amount of computer resources (cpu and memory) is usually required for solution even for flow on a flat plate. Because of the long fetch from the onset of instability to breakdown and the large amplitude ratios associated with this process [$O(e^{Nfactor=10})$ and larger], resolution and bit accuracy limit how far into breakdown that a spatial simulation can go. Because of the large differences in amplitudes throughout the domain and the large growth rates known to exist near breakdown where smaller scales appear, truncation and round-off errors can easily contaminate the solution.

- There is a need to impose a nonintrusive downstream boundary condition since the periodic assumption (associated with temporal simulations) is no longer used. Several ideas have been developed by various investigators. However, there is typically a region of waste where the Navier-Stokes equations are not valid and the solution is discarded. In light of the discussion in (a), this adds to the resource concern.
- The use of either the Nonlinear Parabolized Stability Equations (NPSE; Chapter 4) or DNS simulations, both of which account for nonlinear and nonparallel effects, is hampered by our current lack of knowledge of the connection between the freestream and the boundary-layer response. A physically appropriate upstream or inflow condition must be specified. Efforts to bridge this gap are described in these notes in the section on receptivity.

2.0 NUMERICAL METHODS

The Navier-Stokes equations are highly nonlinear, time-dependent, and elliptic in space. To simulate the spatial evolution of a disturbance field, a numerical method must account for

- time-accurate discretization
- phase-accurate discretization of the convective terms
- sufficient resolution in viscous regions (e.g. close to surfaces and in free shear layers)
- outflow, nonreflective boundary conditions, and (e) efficiency, speed, and "low" memory.

The most highly studied geometry has been the flat plate. Considering the same body-intrinsic coordinate system as in Chapter 4, a finite rectangular box, usually placed downstream of the leading edge and extending from X_o to X_N in the chordwise direction normal to the leading edge, from 0 to Y_N in the direction normal to the surface, and from 0 to Z_N in the spanwise direction parallel to the leading edge, is usually selected as the physical domain. The reaction of this flow to disturbances input along the wall, at the inflow, and/or at the farfield edge of the box is then determined by numerical solution of the complete Navier-Stokes equations for 3-D, time-dependent, compressible or incompressible flow. In this formulation a downstream boundary condition must also be specified.

Different formulations of the Navier-Stokes equations are possible including (for example, in incompressible, Cartesian form):

- Primitive variable with three velocity components u,v,w (in the chordwise x, normal y, and spanwise z directions, respectively) and pressure (four unknown physical quantities).

$$\partial u/\partial x + \partial v/\partial y + \partial w/\partial z = 0$$

$$\partial u/\partial t + \partial u^2/\partial x + \partial(uv)/\partial y + \partial(uw)/\partial z = -\partial p/\partial x + \Delta u$$

$$\partial v/\partial t + \partial(uv)/\partial x + \partial v^2/\partial y + \partial(vw)/\partial z = -\partial p/\partial y + \Delta v$$

$$\partial w/\partial t + \partial(uw)/\partial x + \partial(vw)/\partial y + \partial w^2/\partial z = -\partial p/\partial z + \Delta w$$

where the Laplacian is defined as

$$\Delta = (Re)^{-1} (\partial^2/\partial x^2 + \partial^2/\partial y^2 + \partial^2/\partial z^2)$$

and Re is the Reynolds number based on the freestream velocity U_∞ and a characteristic length l (see below). The restriction to incompressible introduces the computational

difficulty that mass contains only velocity components, and there is no obvious link with the pressure as there is in the compressible formulation through the density. In general, the primitive-variable approach involves using a Poisson equation for the pressure in place of the continuity equation. This is done to separate the majority of the "pressure effects" into a single equation so that the elliptic nature of the flow can be suitably modeled. The pressure Poisson equation is derived by taking the divergence of the momentum equations. The use of a staggered grid permits the coupling of the velocities and pressure at adjacent grid points and can prevent oscillatory solutions, particularly for the pressure, that can occur if centered differences are used to discretize the convective and pressure-gradient terms on a nonstaggered grid. The global coupling implicit in spectral discretization of pressure derivatives can block the appearance of the intertwined but uncoupled pressure solutions associated with centered differences on a nonstaggered grid. A discussion of appropriate boundary conditions for pressure is given by Fletcher (1991), Gresho & Sani (1987), and Gresho (1991).

- Vorticity/stream function (for 2-D only)

$$\partial\omega/\partial t + u\,\partial\omega/\partial x + v\,\partial\omega/\partial y = (Re)^{-1}\,\Delta\,\omega$$

$$\Delta\,\psi = \omega$$

where the Laplacian is defined as

$$\Delta = \partial^2/\partial x^2 + \partial^2/\partial y^2$$

and

$$u = \partial\,\psi/\partial y$$

$$v = -\,\partial\,\psi\,\partial x$$

$$\omega = \partial u/\partial y - \partial v/\partial x$$

and Re is the Reynolds number based on the freestream velocity $U\infty$ and a characteristic length l (see below). The explicit appearance of the pressure is avoided. Two unknown physical quantities are sought and mass conservation does not have to be treated explicitly. The stream-function field must be determined to be compatible with the time-dependent vorticity distribution at every time step. Fletcher (1991) and Gresho (1991) discuss appropriate boundary conditions for the vorticity, as solid-surface boundary conditions are often a weak point.

- Vorticity/velocity with three vorticity-transport equations

$$\partial\omega_x/\partial t + \partial(v\,\omega_x - u\,\omega_y)/\partial y - \partial(u\,\omega_z - w\,\omega_x)/\partial z = (Re)^{-1}\,\Delta\,\omega_x$$

$$\partial\,\omega_y/\partial t + \partial(v\,\omega_x - u\,\omega_y)/\partial x - \partial(w\,\omega_y - v\,\omega_z)/\partial z = (Re)^{-1}\,\Delta\,\omega_y$$

$$\partial\,\omega_z/\partial t + \partial(u\,\omega_z - w\,\omega_x)/\partial x - \partial(w\,\omega_y - v\,\omega_z)/\partial y = (Re)^{-1}\,\Delta\,\omega_z$$

for the vorticity components

$$\omega_x = \partial v/\partial z - \partial w/\partial y$$

$$\omega_y = \partial w/\partial x - \partial u/\partial z$$

$$\omega_z = \partial u/\partial y - \partial v/\partial x$$

and the three Poisson equations for the velocity components

$$\partial^2 u/\partial x^2 + \partial^2 u/\partial z^2 = -\partial\,\omega_y/\partial z - \partial^2 v/\partial x\partial y$$

$$\Delta\,v = \partial\,\omega_x/\partial z - \partial\,\omega_z/\partial x$$

$$\partial^2 w/\partial x^2 + \partial^2 w/\partial z^2 = \partial\, \omega_y /\partial x - \partial^2 v/\partial y \partial z$$

where the Laplacian is defined as

$$\Delta = \partial^2/\partial x^2 + \partial^2/\partial y^2 + \partial^2/\partial z^2$$

and Re is the Reynolds number based on the freestream velocity U_∞ and a characteristic length l (see below). These equations are completed by the conditions of conservation of mass and zero divergence of vorticity

$$\partial u/\partial x + \partial v/\partial y + \partial w/\partial z = 0$$

$$\partial\, \omega_x /\partial x + \partial\, \omega_y /\partial y + \partial\, \omega_z /\partial z = 0$$

There are six unknown quantities to solve.

The analysis is performed by perturbing the complete unsteady Navier-Stokes equations about the basic state. With x, y, and z being the chordwise (tangent to the surface), normal-to-the-wall, and spanwise coordinates, respectively, the Navier-Stokes equations are made dimensionless by introducing a length scale. An appropriate scale taking the y-direction into account is

$$\delta_r = \left(\nu x / U_e \right)^{1/2}.$$

The quantity δ_r is called the local reference boundary-layer thickness. Quantities U_e and ν are the local edge velocity and kinematic viscosity, respectively. Because the goal is a global scheme, representative values of x, say x_0, and U_e, say U_∞, are selected for the length scale l

$$l = \left(\upsilon x_0 / U_\infty \right)^{1/2},$$

and the quantity R, the square root of the x_0-Reynolds number

$$R = \left(x_0 U_\infty / \upsilon \right)^{1/2},$$

is used to represent distance along the surface for the DNS formulation below.

The solution to the Navier-Stokes equations φ consists of two parts, the mean laminar flow solution Φ and the disturbance fluctuation φ',

$$\varphi = \Phi + \varphi'$$

where φ represents the vector of total-flow quantities; for example in the primitive variable form $\varphi = (u, v, w, p, \rho, T, \mu, \lambda, k)$ and u, v, and w are the velocity components in the x, y, and z directions, respectively.

The governing equations can be solved for total-flow quantities (basic state plus disturbance) or disturbance quantities (basic state solved separately) and, if written in conservative form, quantities such as vorticity, energy, etc. are "conserved", even for finite step sizes in the

discretized equations. For transition analysis, equations governing the disturbance are typically solved separately from the basic state. The quantities φ and Φ are each individually solutions to the Navier-Stokes equations, however φ' is not. The basic-state formulations are not presented or discussed here, however the validity of these formulations must also be considered since the transition process is known to be sensitive to subtle changes in the basic state. The numerical accuracy of the basic state must be very high, because the stability and transition results will be very sensitive to small departures of the mean flow from its "exact" shape. The stability of the flow can depend on small variations of the boundary conditions for the basic state, such as freestream velocity or wall temperature. Therefore, basic-state boundary conditions must also be very accurate. See the discussion of Arnal (1994) and Malik (1990).

Because of the need for high spatial resolution, higher than in conventional CFD applications, the use of high-order finite differences and spectral methods is particularly attractive. This is particularly important numerically when trying to advance into regions of large growth rates, small scales, and breakdown. High-order finite-difference and compact methods are attractive because of their enhanced accuracy, relative tolerance of inconsistent boundary conditions, usefulness in complex regions, and resulting matrix structure (banded matrix because they are local methods); these techniques are very popular in spatial-simulation studies. Spectral and pseudospectral methods are global methods requiring less terms in the approximate solution and attractive numerically because of their high accuracy, good resolution in regions of high gradients, and exponential convergence properties and have become popular in transition simulations in various forms. Another advantageous property of these methods is that the energy can be monitored in the coefficients of the higher terms in the series, thus signaling when resolution is inadequate and the simulation must be terminated. Collocation methods are often used for their ease of application, while Galerkin methods can be used in the development of divergence-free basis functions and tau methods may be used when fast solvers are available. However, the issues of incorporating inconsistent boundary conditions, applying spectral methods to complex geometries and compressible flows, and solving flows with discontinuities away from boundaries (Gibbs phenomenon) need to be further addressed. In general, promising active areas of effort include improved iterative convergence and multigrid techniques and spectral domain decomposition and multidomain methods.

One must determine a workable combination of governing equations, boundary conditions, and numerics for each given problem. What works for one situation may not work for another. The available computer, in particular, the architecture, vector length, speed, and memory, also dictates what approach is taken. Thus far, to this author's knowledge, all simulations have assumed periodicity in the spanwise direction and used Fourier series there. (The use of Fourier series allows for the use of Fast Fourier Transforms (FFTs) for the efficient computation of derivatives.)

Investigators are working the prohibitive-computer-resource issue by developing advanced, highly accurate algorithms and the time and memory savings reported by investigators have thus far been encouraging in allowing the spatial simulation to become a more viable tool for the determination of the basic physics. More work to reduce resource requirements for general geometries must be vigorously pursued, however, if spatial simulations are ever to become routine in design.

3.0 DISTURBANCE BOUNDARY CONDITIONS

3.1 Disturbance Input

One advantage of spatial simulations is the freedom and control of what is input as a disturbance; the computation can be made to mimic experiments and provide some guidance. If disturbances are to be introduced directly into the boundary layer along the inflow, typically normal modes from the linear stability theory equation and/or random disturbances have been successfully used. As another example, Singer et al. (1989; temporal simulation) used a combination of random noise and vortices as upstream conditions in the plane channel and showed that, depending on the amplitude of the vorticity, the route to turbulence can be altered and experimental results matched. Alternatively, a periodic suction/blowing (Fasel et al. 1987, 1990) or heater strip (Kral & Fasel 1989, 1990) on the surface will introduce disturbances; this is incorporated into the wall boundary conditions. Spalart (1989, 1990, 1991, 1993) introduces any of random noise, stationary and traveling waves, packets, etc. by means of a body force added to the right-hand side of the momentum equation.

Providing input upstream of the Branch I neutral point of the linear stability curve allows the noise to be washed out of the true disturbance signal in a region of damping before subsequent amplification. All of the above techniques produce linear waves with the appropriate frequency and wavelength, although, the introduction of modes at the upstream boundary requires the smallest downstream distance for this adjustment. However, some of the other techniques can be argued to more mimic the experimental setup.

Alternatively, disturbances can be introduced along the boundaries in the freestream along and/or upstream of the body. For receptivity studies, oscillatory sound and vorticity disturbances are prescribed.

3.2 Freestream Conditions

For incompressible flow, typically the computational box is extended far enough away from the surface to a finite height Y_N to enable the application of decayed-disturbance conditions at the edge; Dirichlet conditions of zero disturbances could be used there, but to eliminate possible reflections from the farfield,

$$\partial q'/\partial y\ (x, z, Y_N) = 0$$

where q' = (u',v',w'), is another possibility. In the case of receptivity, it is possible that an oscillation is provided along some portion of the freestream boundary (see below under receptivity). Fasel & Konzelmann (1990) pointed out that extending the domain to infinity and mapping to a finite domain can add artificial viscosity to the system (Roache 1985), which is very undesirable when the objective is to accurately determine the hydrodynamic stability of a flow.

For supersonic flow, the above conditions can result in spurious reflection from the freestream boundary back into the computational domain. Here one can use a non-reflecting condition (Thompson 1987) based on the inviscid Euler equations containing only the outgoing characteristics.

When the coordinate system for both the basic-state and stability analysis fit the body and bow shock as coordinate lines, linearized Rankine-Hugoniot shock-jump conditions are recommended for the disturbance boundary conditions.

3.3 Wall Conditions

The disturbance may be input to the computational domain along some part of the wall. Otherwise, at the wall, no-slip conditions are used

$$u' = v' = w' = T' = 0$$

If an adiabatic wall is assumed, then

$$\partial T' / \partial y = 0$$

If a 5th condition is needed, either the continuity equation or wall-normal momentum equation can be used. Wall chemistry conditions are discussed in Chapter 13 for hypersonic flows.

3.4 Downstream Boundary Conditions

In disturbance-propagation problems, it is necessary to impose nonreflecting outflow conditions. The elliptic nature of the Navier-Stokes equations comes from two sources: the pressure term and the viscous terms. Interaction of these two effects produces upstream influence; if local velocity perturbations interact with the condition imposed at the downstream boundary, a pressure pulse can be generated that is immediately felt everywhere in the flowfield including the inflow boundary. For example, the popular extrapolation and characteristic conditions applied at the downstream boundary lead to reflections back upstream.

Fasel and colleagues developed the wave condition

$$\partial^2 q'/\partial x^2 = -\alpha^2 q'$$

where α is the dominant streamwise wavenumber and q' is a disturbance quantity. However, unless a single, small 2-D disturbance is the focus of the study, the downstream boundary has to be kept far enough ahead of the disturbance wavefront and the computation stopped before the disturbance hits the downstream boundary to avoid reflections. To quote Fasel et al., "For large growth rates that particularly arise in the leading wave packet, the boundary conditions" above "were not satisfactory and caused strong distortions of the flow field.

The boundary layer is a parabolic, convectively unstable system, where controlled disturbances applied upstream convect downstream and affect transition. But once these disturbances pass by, the boundary layer reverts to its original state before the forcing. As long as sufficient resolution is used and the boundary-layer thickness to streamwise distance is small enough to prevent the transmission of pressure signals over distances of the order of x, advantage can be taken of this property of small upstream influence in formulating the downstream condition.

As one of many examples available in the literature, Streett & Macaraeg (1989) developed a buffer domain. Here a region was appended to the downstream end of the computational domain. In this region, the governing equations were modified to support only downstream-moving waves. By applying the multiplicative factor

$$c(x) = 0.5 \tanh[c_1(L_h - x)] + 0.5$$

- to the streamwise viscous terms $c(x)\,\partial^2 u'/\partial x^2$ to eliminate upstream-influence effects at the boundary
- to the streamwise-perturbation part of the convective velocity $c(x)\,u'\,(\partial U/\partial x + \partial u'/\partial x)$ to eliminate the possibility of advecting streamwise gradients upstream, and
- to the right-hand side of the pressure equation for consistency,

these effects were reduced to zero smoothly with increasing x. Note that when c(x) is zero, the pressure is decoupled from the velocity. [Here, L_h is the half-length of the buffer domain, c_1 is a stretching parameter, x is the streamwise coordinate measured relative to the beginning of the buffer domain, U' is the perturbation velocity vector, u' is the streamwise perturbation velocity, U_b is the base-flow velocity vector.] Joslin et al. (1992a) applied this technique to their fourth-order central-/compact-differencing/spectral code and showed that a buffer region of only three Tollmien-Schlichting (T-S) wavelengths long was sufficient for damping. Obviously, the solution in the buffer region is inaccurate, so that limiting the necessary extent of this region is important.

Other buffer treatments have been proposed and it appears that as long as some sort of reasonable treatment is done downstream ahead of the boundary, the problem of wave reflection back upstream seems to be under control. The major concern is to minimize the wasted region in the computation, in order to keep required resources to a minimum.

4.0 VERIFICATION AND VALIDATION

Here we distinguish between *verification* and *validation*. Per the designations of Roache (1997), we consider verification to mean "confirming the accuracy and correctness of the code" (i.e. is the grid resolved, are there any programming errors in the codes, etc.). Validation requires verification of the code in addition to confirming the adequacy of the equations used to model the physical problem. Strictly speaking, a code can only be validated by comparison with quality experimental data.

There are mainly three sources of error in the abstraction of continuous PDE's to a set of discrete algebraic equations; (1) discretization errors, (2) programming errors (bugs), and (3) computer round-off errors. The objective of code verification is then to completely eliminate programming errors and confirm that the accuracy of the discretization used in solving the continuous problem lies within some acceptable tolerance. Aside from specifying single or double precision, the code developer has little control over the computer round-off errors, but this is usually several orders of magnitude smaller than the discretization error and far less than the desired accuracy of the solution.

In this section we address programming and discretization errors. Many methods are discussed in the literature for code verification using grid refinement, comparison with simplified analytical cases, etc. For recent discussions see Roache (1997) and Oberkampf et al. (1995). Specific suggestions for testing a CFD code for the study of transition include (a) grid-refinement studies, (b) solving test problems for which the solution is known, (c) changing the "far-field" boundary locations systematically and re-solving, (d) comparing linear growth rates, neutral points, and eigenfunctions with linear stability theory, (e) running the unsteady code with time-independent boundary conditions to ensure that the calculations remain steady, and (f) running geometrically unsymmetric codes with symmetric conditions.

In addition to the usual code verification techniques, there is a general method to verify the discretizations and locate programming errors by comparison with "manufactured" analytical solutions (Steinberg & Roache, 1985). This method is general in that it can be applied to any system of equations. Although it is an extremely powerful tool, this method has received relatively little attention in the literature. For clarity the technique is demonstrated on the Poisson equation.

$$Lu \equiv \frac{\partial^2 u}{\partial x^2} + \frac{\partial^2 u}{\partial y^2} = F(x, y)$$

To solve this problem, discretize the operator L using some appropriate approximation (finite differences, spectral, etc.). In general, the exact solution is not available. Therefore, for verification purposes, *force* the solution to be some combination of analytical functions with nontrivial derivatives. For example, consider the system $g \equiv Lv = 5e^{3y}\sin(2x)$, which has an analytical solution $v = e^{3y}\sin(2x)$. The exact solution can then be compared with the computed solution. Of course, manufactured solutions should be chosen with topological qualities similar to those anticipated for the solution to the "real" problem (e.g. gradients close to the wall). Proper choice for the manufactured solutions also allows the discretization of the boundary conditions to be verified. For large systems of equations a symbol manipulator is recommended for computing g. If a bug occurs, zeroing the coefficients of some terms in the equation can help to isolate the bug.

Validation is defined as encompassing verification of the code as well as confirming that the equations used to model the physical situation are appropriate. The basis of validation is assumed to be a successful comparison with the few careful, archival experiments available in the literature. To date the DNS have been successfully validated for a variety of 2- and 3-D flow situations.

5.0 BASIC PHYSICS AND VALIDATION

In this section, we outline progress in DNS studies of receptivity and mechanisms for unswept flowfields.

5.1 Receptivity

In spite of progress, an overall theory remains rather incomplete with regard to predicting transition. Amplitude and spectral characteristics of the disturbances inside the laminar viscous layer strongly influence which type of transition occurs. Thus, it is necessary to understand how freestream disturbances are entrained into the boundary layer and create the initial amplitudes of unstable waves, i.e., to answer the question of receptivity.

External disturbances common to the flight environment are typically either acoustic or vortical. These types of disturbances are referred to as natural disturbances. In contrast, disturbance environments produced by artificial means such as a vibrating ribbon or suction & blowing are referred to as forced disturbances. Whereas forced disturbances typically contain a broadband of wavelengths, naturally occurring disturbances typically have a narrow wavelength band. The important distinction is that acoustic waves or vortical disturbances generally will not contain a wavelength that coincides with the instability that is generated within the boundary layer. Thus in this case some mechanism for transferring energy from a much longer wavelength wave to a relatively small wavelength instability wave must exist.

For the discussion here, the focus is on 2-D boundary layers and the ultimate goal is to determine how the wave amplitude within the boundary layer can be found from a freestream measurement. Since receptivity deals with the generation rather than the evolution of instability waves in a boundary layer, neither departures from the linear-mode scenario nor details of the transition process itself are discussed here.

For incompressible flows, receptivity has many different paths through which to introduce a disturbance into the boundary layer. These include the interaction of freestream sound or turbulence with leading-edge curvature, discontinuities in surface curvature, or surface inhomogeneities. Moreover, the picture for 3-D flows is expected to be different than that of 2-D flows. Essentially, the incoming freestream disturbance at wavenumber α_{fs} interacts with a non-homogeneity of the body causing its spectrum to broaden to include the response wavenumber α_{TS}. Small initial amplitudes of the disturbances tend to excite the linear normal modes of the boundary layer which are of the T-S type (Mack 1984).

It is believed that the *vortical* parts of the freestream disturbances (turbulence) are the contributors to the 3-D aspects of the breakdown process (Kendall 1984, 1998) while the *irrotational* parts of the freestream disturbances (sound) contribute to the initial amplitudes of the 2-D T-S waves Kosorygin et al (1995). Thus, freestream sound and turbulence present a different set of problems in the understanding, prediction, and control of boundary transition and, as such, each require unusual experimental and computational techniques.

In this section we focus on recent DNS simulations of leading-edge effects and confine our discussion to incompressible flow. A review of the earlier computational efforts is given by Saric et al (1994, 1999, 2002) and is not repeated here. This is a critical area in need of validation where spatial DNS can excel if the community is to begin to accurately model how the freestream relates to the transition mechanisms observed in the boundary layer and ultimately predict transition location.

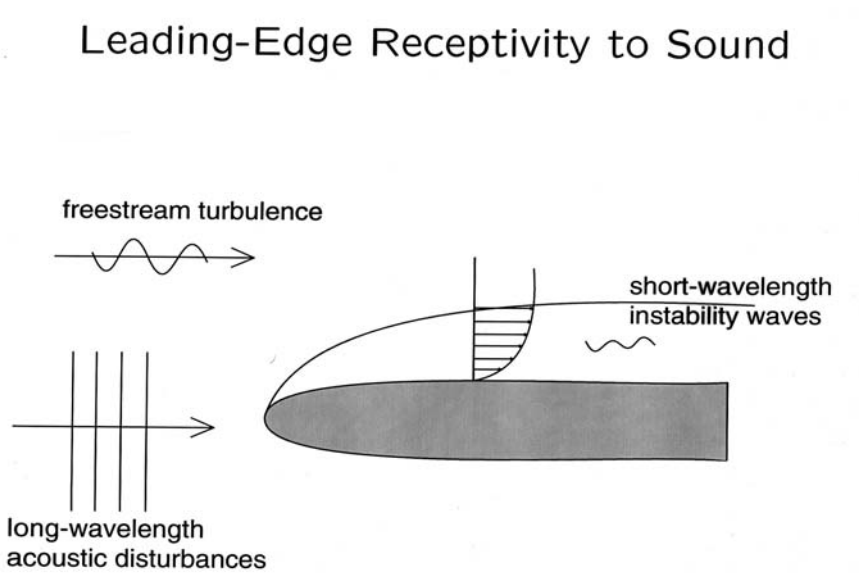

5.1.1 DNS of Leading-Edge Receptivity to Freestream Sound

Theoretical Basis. Theoretical investigations into acoustic receptivity have blazed the trail in our understanding and identified mechanisms for the transfer of energy among disparate wavelengths. In the research of Lam & Rott (1960), Ackerberg & Phillips (1972), and Goldstein (1983), receptivity to acoustic waves impinging upon a flat-plate geometry at zero angle of incidence was investigated. The primary mechanism for transferring energy is the relatively rapid growth of the mean boundary layer and the associated pressure gradients near the stagnation point. The investigations were performed using the Linearized Unsteady Boundary Layer Equation (LUBLE) which is a parabolic equation and therefore conducive to less costly numerical methods. Energy from the external disturbance environment is transferred to streamwise decaying eigenfunctions whose wavelength decreases as the flow progresses downstream. Thus a process by which long wavelengths become shorter wavelengths is found in these so called Lam-Rott eigenfunctions. The Lam-Rott eigenfunctions match onto solutions of the linear stability theory downstream. Therefore if one knows the amplitude of the Lam-Rott eigenfunction the amplitude of the instability wave downstream is known. Goldstein et al. (1983) and Heinrich & Kerschen (1989) calculated leading-edge receptivity coefficients for various freestream disturbances. Goldstein (1985) and Goldstein & Hultgren (1987) also showed that discontinuities in slope or curvature in the geometry also provide a mechanism for acoustic receptivity. Regions where surface irregularities exist promote small-scale variations of the mean-flow boundary layer and therefore the mechanism is very similar to the flat-plate case with no surface irregularity.

Heinrich et al. (1988) applied the LUBLE to acoustic waves at varying angles of incidence impinging upon a flat plate. The results produced show a strong dependence of initial amplitude of the instability wave on the angle of incidence of the impinging acoustic wave. In addition, the effect of angle of incidence is found to be more pronounced for smaller Mach numbers and singular in the limit as the Mach number approaches zero.

The above results apply to a zero-thickness flat plate. Hammerton & Kerschen (1996, 1997) extend the analysis to account for a finite-thickness and -curvature leading edge by considering a parabolic geometry. The analysis is formulated to provide insight into the effect of nose radius, an effect present in any manufacturable geometry. The Mach number and the amplitude of the impinging acoustic disturbance are considered to be small, so that the mean-flow pressure field can be computed with incompressible theory. The mean flow is two-dimensional and symmetric. Lam & Rott (1993) generalize their eigenfunctions to account for arbitrary streamwise variation in the mean flow, and Hammerton & Kerschen (1996) show that their expressions are in agreement with these more general results. The relevant parameter is the Strouhal number based on the nose radius St_r. The results of this work show that the receptivity coefficient is nearly unity when the nose radius is zero and decreases dramatically with increasing nose radius. The receptivity coefficient is shown to increase with increasing angle of incidence of the acoustic wave. Hammerton & Kerschen (1997) consider the small-Strouhal-number limit. For freestream acoustic waves at zero incidence, the receptivity is found to vary linearly with Strouhal number, giving a small increase in the receptivity coefficient relative to that for the flat-plate case. However, for oblique waves, the receptivity varies with the square root of the Strouhal number, leading to a sharp decrease in the amplitude of the receptivity coefficient compared to the flat-plate case.

Experiments. A leading edge with finite curvature and thickness has been shown to produce instability waves. Experiments in leading-edge receptivity have shown that great care must be taken in order to produce results that are comparable to theory and numerical simulation (Saric 1994). The very small amplitudes upstream are not detectable in the experiments and the

instability waves can only be measured after significant growth has occurred. However, once the amplitude of an instability wave has been determined downstream one can use linear stability theory to provide amplitudes in the leading-edge region.

Receptivity Coefficient. Receptivity results can be expressed either in terms of

- a leading-edge receptivity coefficient defined as the ratio of the T-S amplitude in the leading-edge region at $x = O(U_\infty / 2\pi f)$ to the freestream-sound amplitude:

$$K_{LE} = \left|u'_{TS}\right|_{LE} \Big/ \left|u'_{ac}\right|_{fs} \qquad (1)$$

or

- a Branch I receptivity coefficient defined as the T-S amplitude at Branch I normalized with the freestream-sound amplitude

$$K_I = \left|u'_{TS}\right|_I \Big/ \left|u'_{ac}\right|_{LE} \qquad (2)$$

where $|\ |$ denotes absolute value or rms.

Haddad & Corke (1998) argue that the appropriate receptivity coefficient is Equation (1), the one that uses the T-S amplitude at the leading edge, $\left|u'_{TS}\right|_{LE}$, instead of $\left|u'_{TS}\right|_I$. The advantage is that one can define the receptivity coefficient, K_{LE}, based strictly on local properties of the leading-edge region, whereas $\left|u'_{TS}\right|_I$ and K_I depend on the pressure gradient history from the leading edge to Branch I. Moreover, K_{LE} decreases with nose radius and K_I increases with nose radius which could lead to some confusion.

These arguments are compelling, but utilitarian issues argue for the use of Equation (2). For example:

- it is impossible for an experiment to measure $\left|u'_{TS}\right|_{LE}$
- most transition correlation schemes begin with Branch I calculations
- the pressure gradient history can easily be accounted for by linear stability theory calculations up to a region near the leading edge.

The author strongly urges that Equation (2) be adopted as the accepted measure of receptivity.

DNS Validation. With the spatial computational method, finite curvature can be included in the leading-edge region. *This feature was left out of some early unsuccessful receptivity models.* Lin et al (1992) demonstrated that as the aspect ratio of the elliptic nose on a flat plate is sharpened from 3 (blunt) to 9 to 40 (very thin) and the vorticity tends to become singular. By stipulating the plate to have finite curvature at the leading edge, the singularity there is removed and a new length scale is introduced.

Experimentally, the most popular model geometry for receptivity has been the flat plate with an elliptic leading edge. Thus it is reasonable that computational models consider the same geometry. However, the curvature at the juncture between the ellipse and the flat plate is discontinuous and provides a source of receptivity (Goldstein 1985; Goldstein & Hultgren 1987).

Lin et al (1992) introduced a new leading-edge geometry based on a modified super-ellipse (MSE) given by

$$[(a-x)/a]^{m(x)} + [y/b]^n = 1, \quad 0 < x < a$$

$$m(x) = 2 + [x/a]^2 \text{ and } n = 2$$

where $a = b(AR)$, b is the half-thickness of the plate, and AR is the aspect ratio of the "elliptic" nose. For a usual super-ellipse, both m and n are constants. These super-ellipses will have the advantage of continuous curvature (zero) at the juncture with the flat plate as long as $m > 2$ at $x/b = AR$. The MSE, with $m(x)$ given above, has the further advantage of having a nose radius and geometry (hence a pressure distribution) close to that of an ordinary ellipse.

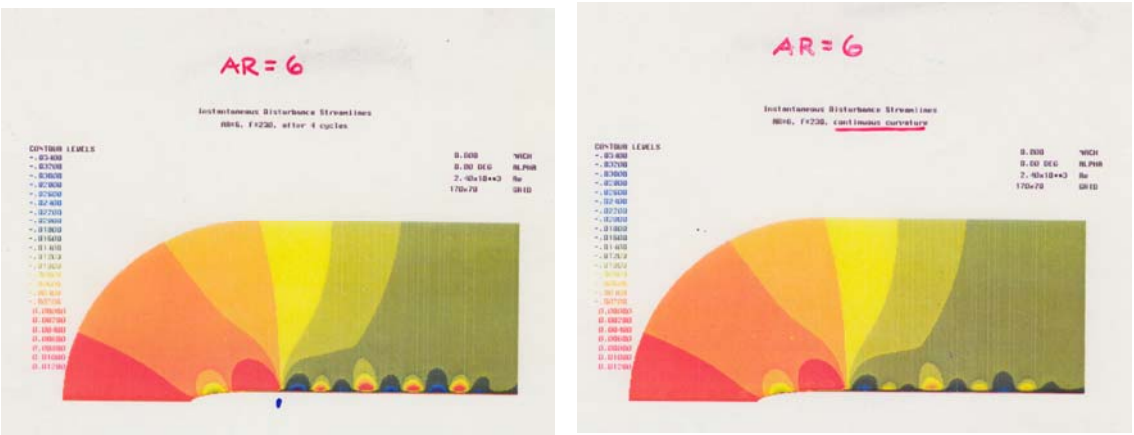

Figure 2. Lin et al. (1992) demonstrated that when the discontinuity in curvature at the ellipse/flat-plate juncture (left figure) was faired by a polynomial (right figure), receptivity was cut in half. Note the colors in the figure on the right are less intense downstream near the wall. The aspect ratio of the elliptic leading edge is 6.

Lin et al (1992) simulated the receptivity of the laminar boundary layer on a flat plate by solving the full Navier-Stokes equations in general curvilinear coordinates. They used a *C*-type orthogonal grid and included the finite-thickness leading edge and curvature. Geometries tested included elliptic, polynomial-smoothed elliptic, and MSE leading edges of different aspect ratios. Various sound-like oscillations of the freestream streamwise velocity were applied along the boundary of the computational domain and allowed to impinge on the body. Parameters that were varied included disturbance amplitude and frequency, as well as leading-edge radius and geometry. They found the following:

- T-S waves appearing in the boundary layer could be linked to sound present in the freestream.
- Receptivity occurred in the leading-edge region where rapid streamwise adjustments of the basic flow occurred.
- The magnitude of receptivity and the disturbance response depended very strongly on geometry. For example:

- For plane freestream sound waves, T-S wave amplitude at Branch I decreased as the elliptic nose was sharpened. However, this is due to the relaxation of the adverse pressure gradient
- When the discontinuity in curvature at the ellipse/flat-plate juncture was faired by a polynomial, receptivity was cut in half
- The disturbance originated from the location of the maximum in adverse pressure gradient.

- The receptivity to plane freestream sound appeared to be linear with freestream-disturbance amplitudes up to about 5% U_∞. Thus, a linear Navier-Stokes solution could be used up to these levels.

Fuciarelli et al (2000) and Wanderly & Corke (2001) obtain receptivity coefficients for a 20:1 MSE over a range of frequencies that can be compared with the experiments of Saric & White (1998). The results are shown in Table 1. The receptivity coefficient, K_I, is as defined above in Equation (2) referencing the Branch I neutral stability point. The receptivity coefficients have been extrapolated downstream from the numerical results by using linear stability theory. The results of the numerical simulations show no significant variation with frequency. The agreement between the computations and the experiment is excellent, and we conclude that each validates the other. One notes that the experiment is exceptionally difficult and requires very special care.

TABLE 1: Branch I receptivity coefficients for multiple frequencies as predicted by DNS and compared with the experiments.

	Wanderley & Corke (2001)	Fuciarelli et al (2000)	Saric & White (1998)
Case	DNS	DNS	Experiment
F	90	82—86	88—92
K_I	0.046	0.048	0.050 ± 0.005

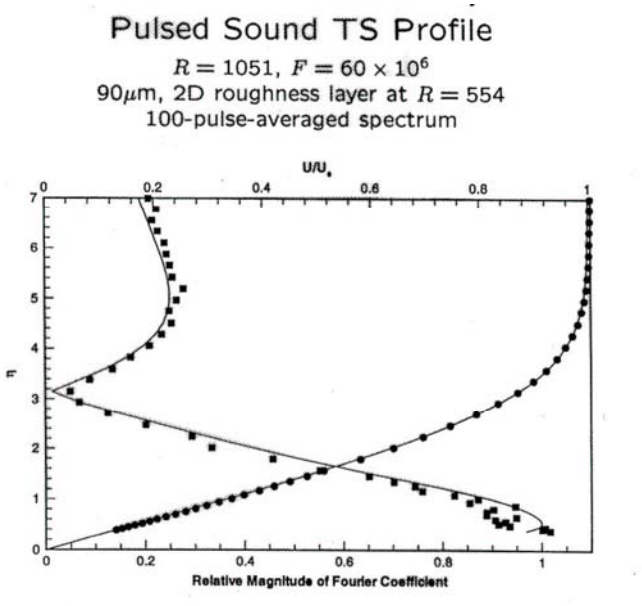

Figure 3. Saric & White (1998) demonstrate that their experimentally measured disturbance mode indeed matches that predicted by LST.

Wanderly & Corke (2001) extend the computations over the frequency spectrum at the same Reynolds number for the case of different leading edge shapes. This is an extraordinarily useful result. Not only does one have the Branch I initial amplitude for an amplification factor calculation (given a freestream measurement) but also a very good example of how a leading-edge design needs to proceed.

In the case of receptivity, theory has led the way in our understanding. Here the DNS results are compared with the theoretical predictions of Goldstein (1983), Kerschen et al (1990), and Hammerton & Kerschen (1996) where the leading-edge receptivity coefficient is found to be approximately 0.95 (Equation 1). The results of Haddad & Corke (1998) show that the leading-edge receptivity coefficient has a value of approximately 0.47 for a Strouhal number, $S = r_n 2\pi f/U_\infty$, of 0.01. Using the same Strouhal number, Fuciarelli et al (2000) march upstream to an x-location of 1/2 the wavelength of the associated instability wave [which approximates the LUBLE region defined by $x2\pi f/U_\infty = O(1)$] and predict a leading-edge value of approximately 0.75. In an improved calculation, Erturk & Corke (2001) predict K_{LE} = 0.64 at S = 0.01 and K_{LE} = 0.76 at S = 0. All of the computations show a strong decrease in K_{LE} with an increase in S in agreement with theory. In trying to do these comparisons, certain difficulties arise and hence the differences between the calculations is purely technical. The major uncertainty that exists in the DNS (and experiments) is the use of K_{LE} and the choice of streamwise location in the leading-edge region at which the amplitude should be sampled for comparison with the asymptotic theory. However crude these comparisons may be, it is clear that the essential ideas of the asymptotic theory have been verified experimentally and computationally.

5.1.2 DNS of Leading-Edge Receptivity to Freestream Sound at Angle of Incidence

Acoustic waves impinging upon the leading edge at angles of incidence αac were studied numerically by Haddad & Corke (1998), Fuciarelli et al (2000), and Erturk & Corke (2001). The comparisons among the three are difficult for a number of reasons. The computations have a semi-infinite body and the theory has a finite chord. Haddad & Corke (1998) vary both body and incident sound angle of attack while Fuciarelli et al (2000) fix the body and vary the incident sound angle. Nevertheless some highlights are relevant.

Non-symmetric forcing of the acoustic wave yielded an increase in the leading-edge receptivity coefficient with increasing angle of incidence but at a much smaller rate than that predicted by the theory for the zero-thickness flat plate. The slope of the increase in receptivity for the DNS is approximately 0.15 whereas the increase as predicted by Heinrich & Kerschen (1989) is about 0.65. The DNS predicts a slope of less than 1/4 of the slope predicted by this theory.

A comparison with the finite-nose-radius theoretical results of Hammerton & Kerschen (1996, 1997, 2000) shows much more encouraging results. Fuciarelli et al (2000) use an Ansatz (details are in the paper) for finite chord and developed the following comparison of KLE at S = 0.01.

TABLE 2: Leading-edge receptivity coefficients for various incidence angles as predicted by DNS and compared with the finite-nose-radius theory.

	Fuciarelli et al (00)	Hammerton & Kerschen (96)
α_{ac} (degrees)	K_{LE} DNS	K_{LE} Theory
0	0.75	1.0
5	1.3	1.8
10	2.1	2.6
15	3.2	3.4

The agreement is excellent and clearly demonstrates the importance of including the effects of the finite nose radius in any receptivity study.

5.1.3 Receptivity to freestream vorticity

The characteristic length scale for freestream vorticity is the convective wavelength $U_\infty/2\pi f$, which is approximately 3 times that of the amplified T-S wave at that frequency.

The Kendall Experiment. Over the past 20 years, Kendall has developed careful and well-thought-out experimental setup where the freestream turbulence can systematically be controlled and initiation of T-S waves in the boundary layer can be examined. The specific goal of these experiments was to relate T-S wave amplitude to measured freestream turbulence amplitude.

In contrast to acoustic forcing, freestream turbulence initiates three distinct motions within the boundary layer. The first motion is a sustained, streaky $(z \approx 2\delta)$, high amplitude $(|u'| \approx 5-10\%\ U_\infty)$ motion, which is probably due to stretching of the ingested freestream vorticity and the growth of transient modes. This is historically called the Klebanoff mode. The second is an outer-layer oscillation at T-S frequencies that grows weakly in the stream direction. These modes may have some connection with the continuous spectrum of the linear stability theory, but this is not clear. The third is the usual T-S mode, which exhibits higher growth rates.

The KTH Experiments. The KTH experiments had as their goal the determination of the role of transient growth.

- The boundary layer responds nonlinearly to an increase in freestream turbulence as first shown by Kendall. Again there is the conjecture that there is a continuous receptivity process along the streamwise extent of the boundary layer.
- Transient (algebraic) growth plays a more important role in the boundary layer response as freestream turbulence is increased. Referring back to the Roadmap, the path to transition for the lowest freestream disturbance levels (A) does not include transient growth. As the freestream amplitude is increased, a point is reached where the primary linear stability theory modes are bypassed completely.
- Transient growth plays a particularly strong role in the presence of distributed surface roughness.
- As with Kendall experiments, the coupling coefficient has not been determined.

DNS Validation. Buter & Reed (1994) simulated the receptivity of the laminar boundary layer on a flat plate by solving the full Navier-Stokes equations in general curvilinear coordinates using the same techniques and geometries as Lin et al (1992). A simple model of time-periodic freestream spanwise vorticity was introduced at the upstream computational boundary. This signal was decomposed into a symmetric and asymmetric streamwise velocity component with respect to the stagnation streamline. The computations were performed with these individual components specified as boundary conditions so that for small disturbances, the results could then be linearly superposed. Moreover, the effect of a transverse-velocity component at the leading edge could be ascertained as the asymmetric-velocity case had this feature while the symmetric-velocity did not. They found the following:

- As the disturbance convected past the body, it was ingested into the upper part of the boundary layer, decaying exponentially toward the wall. This was consistent with the findings of Kerschen (1989) and Parekh et al (1991).
- Different wavelengths were evident in the boundary-layer response. Signals at the T-S wavelength were dominant near the wall, while toward the edge of the boundary layer, disturbances of the freestream convective wavelength were observed. This was consistent with the experimental observations of Kendall (1991).
- T-S waves appearing in the boundary layer could be linked to freestream vorticity acting near the basic-state stagnation streamline.
- For the particular geometric and flow conditions considered in this study, receptivity to vorticity was found to be smaller than receptivity to sound by a factor of approximately three.
- Modifications to the geometry which increased the surface pressure gradient along the nose increased receptivity.
- For both the symmetric and asymmetric freestream velocity perturbations, the T-S response was linear with forcing over the range of amplitudes considered; symmetric: up to 4.2% U_∞ and asymmetric: up to 2.1% U_∞.
- A superharmonic component of the disturbance motion was observed at all forcing levels for the asymmetric forcing. This was initially observed in the stagnation region where the interaction of the asymmetric gust with the basic flow induced a large transverse velocity component which interacted with the adverse pressure gradient upstream of the nose to transfer disturbance energy to the superharmonic frequency.

5.1.4 Observation

The past decade has seen considerable progress in the understanding of receptivity mechanisms. The agreement among theory, computations, and experiment on leading-edge receptivity and 2-D roughness (although not discussed here) is remarkable. DNS has been established as a viable framework for more detailed studies on different geometries. Challenges still exist in the areas of freestream turbulence, transient growth, and bypasses. We expect progress to occur when theoretical, computational, and experimental methods are combined to address these important problems.

For each configuration under consideration, the complete integrated picture of geometry and associated pressure gradients (both favorable and adverse) must be included in any meaningful evaluation of receptivity, and it is here that computations by spatial DNS can excel. A variety of different freestream disturbances can be implemented with this technique and the response of the boundary layer quantified and catalogued. Moreover, these results begin to provide the link between the freestream and the initial boundary-layer response and can provide the upstream conditions for further DNS or Parabolized Stability Equation (PSE) simulations accurately marching through the transition process toward turbulence.

5.2 Secondary Instabilities and Transition Mechanisms in 2-D Boundary Layers

There are different possible scenarios for the transition process, but it is generally accepted that transition is the result of the uncontrolled growth of unstable 3-D waves. In this section, the reader is only glimpsing the kinds of problems that the DNS has and can tackle in our quest to understand, predict, and control transition. It proves to be a powerful tool in helping sort out the physical mechanisms at work.

5.2.1 Fundamental Mode Breakdown

The occurrence of 3-D phenomena in an otherwise 2-D flow is a necessary prerequisite for transition (Tani 1981). Such phenomena were observed in detail by Klebanoff et al. (1962) and were attributed to a spanwise differential amplification of T-S waves through corrugations of the boundary layer. The process leads rapidly to spanwise alternating "peaks" and "valleys", i.e., regions of enhanced and reduced wave amplitude, and an associated system of streamwise vortices. The peak-valley structure evolves at a rate much faster than the (viscous) amplification rates of T-S waves. This represents the path to transition under conditions similar to Klebanoff et al. (1962) and is called a K-type breakdown. The lambda vortices are ordered in that peaks follow peaks and valleys follow valleys. Since the pioneering work of Nishioka et al. (1975, 1980), it is accepted that the basic transition phenomena observed in plane channel flow are the same as those observed in boundary layers. Therefore, little distinction will be given here as to whether work was done in a channel or a boundary layer. From the theoretical and computational viewpoint, the plane channel is particularly convenient since the Reynolds number is constant, the mean flow is strictly parallel, certain symmetry conditions apply, and one is able to apply temporal theory. Thus progress was first made with the channel-flow problem.

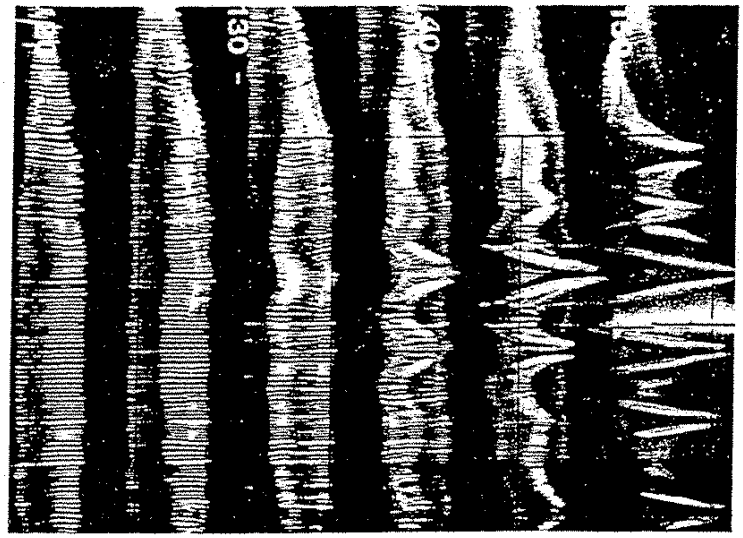

Figure 4a. Visualization of K-type breakdown (Saric 1986). Flow is from left to right.

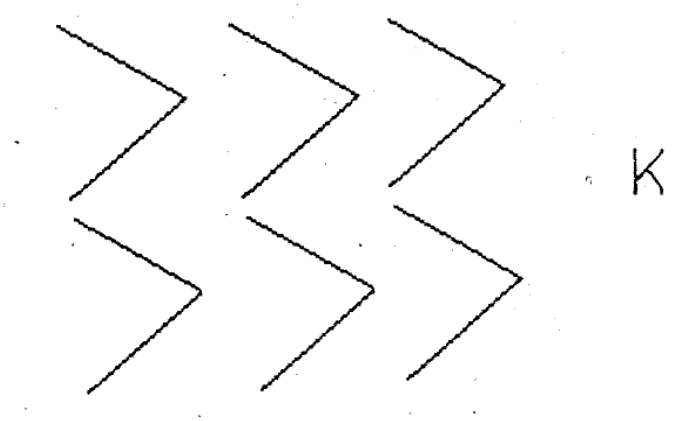

Figure 4b. Sketch depicting K-type breakdown. Flow is from left to right.

5.2.2 Subharmonic Mode Breakdown

Different types of 3-D transition phenomena observed (Saric & Thomas 1984, Kachanov et al. 1977, Thomas & Saric 1981, Kachanov & Levchenko 1984, Saric et al. 1984, Kozlov & Ramazanov 1984) are characterized by staggered patterns of peaks and valleys and by their occurrence at very low amplitudes of the fundamental T-S wave. This pattern also evolves rapidly into transition. Hot-wire measurements in these experiments show that the subharmonic of the fundamental wave (a necessary feature of the staggered pattern) is excited in the boundary layer and produces either the resonant wave interaction predicted by Craik (1971; called the C-type) or the secondary instability of Herbert (1984; called the H-type). Spectral broadening to turbulence with self-excited subharmonics has been observed in acoustics, convection, and free shear layers and was not identified in boundary layers until the preliminary results of Kachanov et al. (1977). This paper re-initiated the interest in subharmonics and prompted the simultaneous verification of C-type resonance (Thomas & Saric 1981, Kachanov & Levchenko 1984). Subharmonics have also been confirmed for channel flows (Kozlov & Ramazanov 1984) and by direct integration of the Navier-Stokes equations (Spalart 1984, Spalart & Yang 1987).

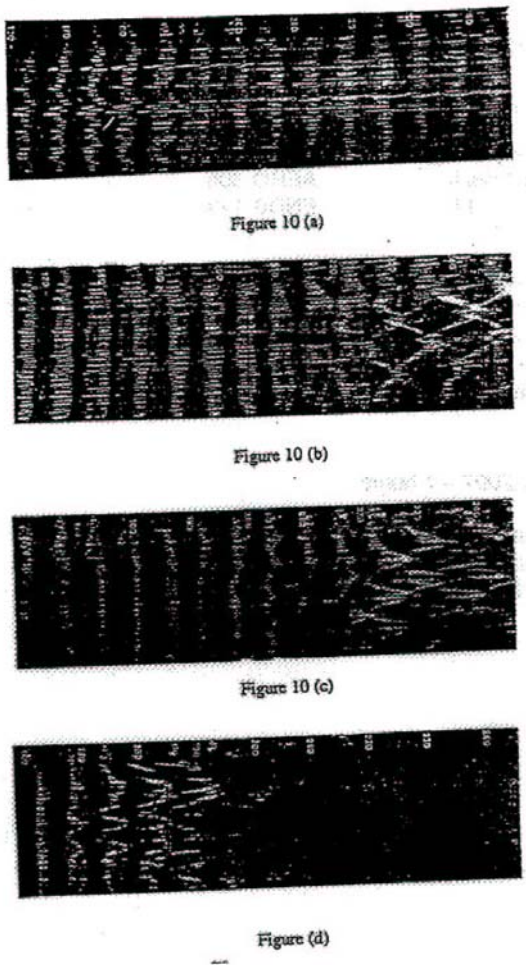

Figure 5a. Experimental visualization of different transition mechanisms on a flat plate. Successive images (top to bottom) represent the same operating conditions on the same flat plate in the same quiet wind tunnel, but with increasing introduced initial disturbance amplitude. Figures (a) – full laminar flow, (b) Craik-type or C-type triad resonance, (c) Herbert-type or H-type subharmonic breakdown, (d) Klebanoff-type or K-type breakdown. *Note the very significant differences in the transition location due to differences in upstream conditions and associated breakdown processes.* Flow is from left to right. From Saric (1986).

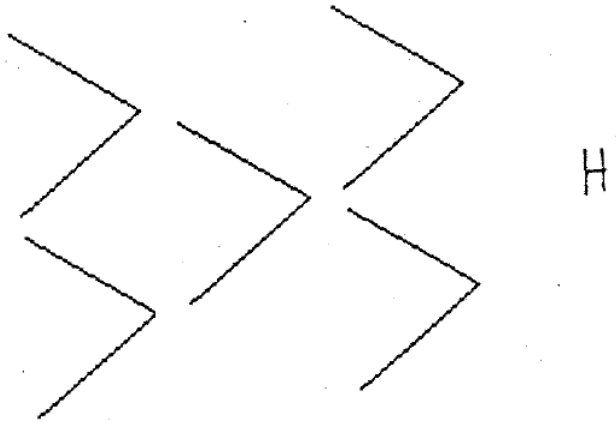

Figure 5b. Sketch depicting H-type breakdown. Flow is from left to right.

Corke & Mangano (1989) and Corke (1994) introduced controlled 3-D subharmonics alongwith the 2-D fundamental. Only then could detailed measurements be made of the disturbance flow field. By using segmented heating elements, it is possible to phase shift a signal to each element and create an oblique wave at any angle or frequency. Then the 2-D fundamental and the 3-D subharmonic are a simple electronic superposition (Corke 1994). As a result, the Corke subharmonic experiments contain the most complete and reliable set of data on subharmonic breakdown. Both chordwise and spanwise variations of the fundamental and subharmonic are given. Corke (1990) gives several possible interactions. Another example of the richness of this work are the disturbance streamlines that are reconstructed from numerous profiles. These measurements are taken at different chord locations but at the same point in the oscillation cycle. One sees an increase in intensity toward the wall as the measurements move downstream. These are data that will positively challenge and validate the NPSE and DNS work. The space in this report is not sufficient to cover all of the different types of behavior that are part of the subharmonic breakdown process. The reader is encouraged to go to the original references.

5.2.3 Direct Numerical Simulation.

A surprise that results from the analytical model of Herbert (1984) and the Navier-Stokes computations of Singer et al. (1986, 1989), is that under amplitude conditions of the experimentally observed K-type breakdown, the subharmonic H-type is still calculated to be the dominant breakdown mechanism instead of the fundamental mode. This is in contrast to Klebanoff's experiment, confirmed by Nishioka et al. (1975, 1980), Kachanov et al. (1977), Saric & Thomas (1984), Saric et al. (1984), and Kozlov & Ramazanov (1984) where only the breakdown of the fundamental into higher harmonics was observed. Only Kozlov and Ramazanov observed the H-type in their channel experiments and only when they artificially introduced the subharmonic.

This apparent contradiction was resolved by Singer et al. (1989). Under the conditions of a forced 2-D, T-S wave and random noise as initial conditions, the subharmonic mode is present as predicted by theory but not seen experimentally. However, when streamwise vorticity (as is present in the flow from the turbulence screens upstream of the nozzle) is also included, the subharmonic mode is overshadowed by the fundamental mode (as in the experiments!). When streamwise vortices are included with the theoretical parabolic shape, the resulting pattern is an ordered peak-valley structure. Here is a case in which the computations have explained

discrepancies between theory and experiments. In the presence of streamwise vorticity, the fundamental mode is preferred over the subharmonic; this agrees with experimental observations, but not with theory (which does not account for this presence). Without streamwise vorticity, the subharmonic modes dominate as predicted by theory and confirmed by computational simulations. In the presence of streamwise vorticity characteristic of wind-tunnel experiments, the K-type instability dominates and the numerical simulations predict the experimental results. Thus, each experiment is naturally contaminated with low-level streamwise vorticity that provides the background 3-D that leads to the secondary instabilities. Moreover, ongoing developments in studies of transient growth promise to put the role of streamwise vorticity on a firm footing; see the section on transient growth.

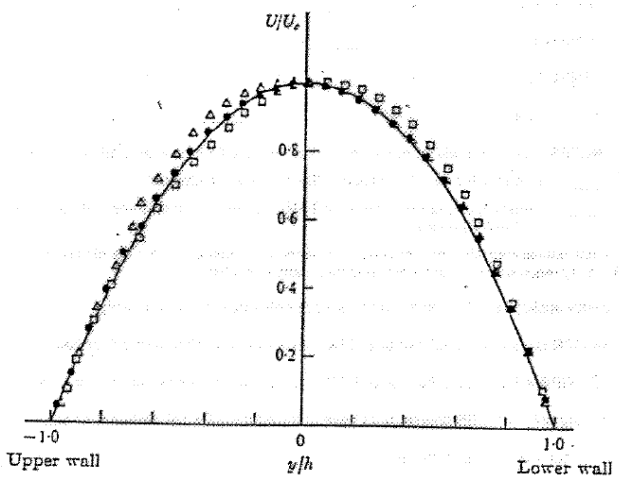

Experimental measurements of streamwise velocity at various spanwise positions in Poiseuille flow channel (Nishioka et al. 1975)

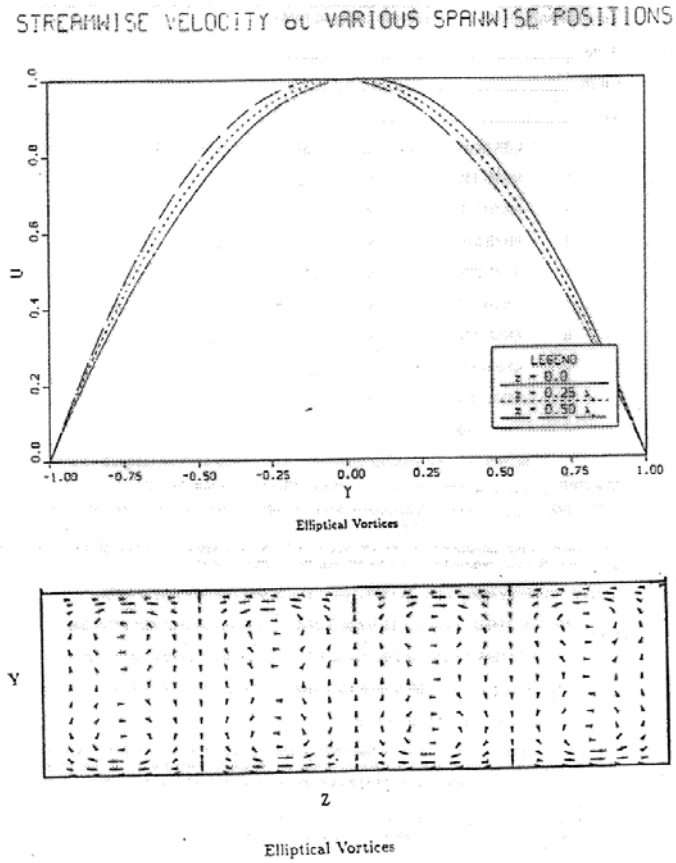

Figure 6. Computations including streamwise vorticity in Poiseuille flow channel (Singer et al. 1989)

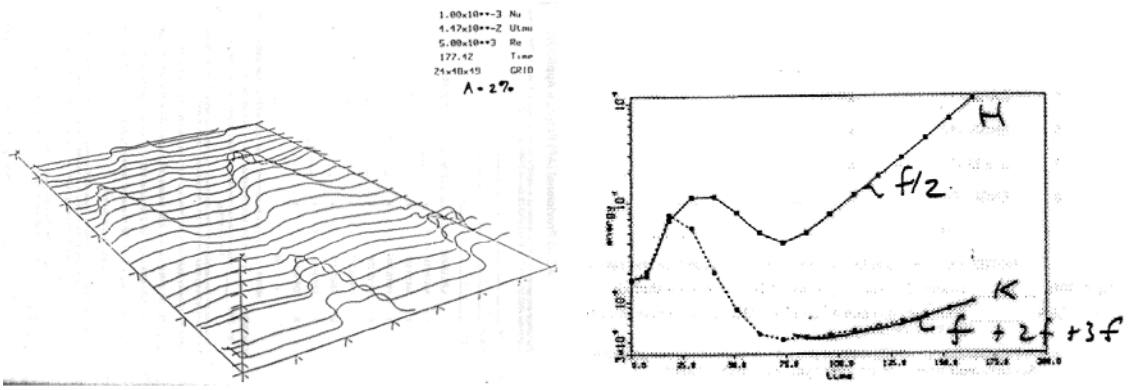

Figure 7. DNS of plane Poiseuille with forcing of fundamental and random noise shows H-type breakdown. Under same flow conditions, experiment shows K-type breakdown

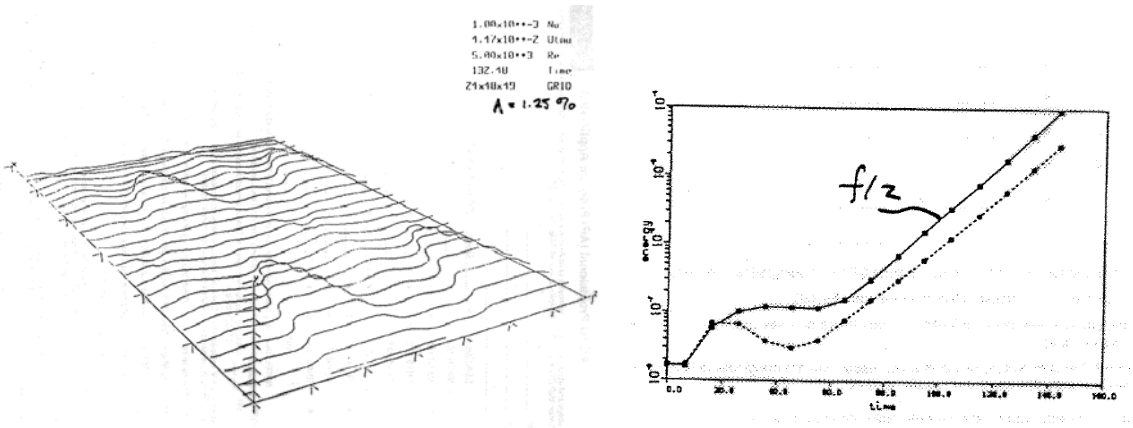

Figure 8. DNS of plane Poiseuille with forcing of fundamental, streamwise vortices, and random noise shows K-type breakdown. Under same flow conditions, experiment shows K-type breakdown.

Computations by Fasel et al. (1990) and Fasel (1990) under the conditions of Klebanoff et al. (1962) showed poor agreement of the spatial growth at peak and valley stations, until a small streamwise pressure gradient was added to the computations. This pressure gradient was present in the experiments of Klebanoff et al. Rist & Kachanov (1995) made very detailed comparisons of the results of hot-wire measurements and DNS for K-type breakdown and showed very good agreement of the spatial disturbance development, the disturbance spectra, the instantaneous velocity traces, and the local frequency/spanwise-wavenumber spectra. By detailed quantitative comparisons of experimental measurements and results of DNS, they have generated a validated data base that may be used for the validation of different theories.

Joslin & Streett (1992) simulated the subharmonic experiments of Kachanov & Levchenko (1984) and found good qualitative agreement. There were some modal discrepancies observed between the two, though, which were resolved when the computations included a small adverse pressure gradient and a small effective frequency variation in the disturbance.

5.2.4 Point-Source Disturbances

Another important class of experiments deals with the point source within the boundary layer as a generator of 3-D disturbances. The classical experiment in this area is that of Gaster & Grant (1975). In this work, wave packets are created by impulse disturbances that are introduced at the wall. The initial impulse excites many different modes which are selectively amplified and can undergo interference within the boundary layer. Thus one sees a 3-D packet of waves that grows and spreads in the flow direction. The idea is that this is a model of "natural" disturbance generation within the boundary layer with which many common features are shared. Gaster & Grant (1975) show a series of hot-wire traces at different downstream distances along the centerline and the shape of the disturbed region is shown in contour plots. Wavenumber-frequency data are also given with enough detail as to provide the grist for the theoretician's mill. See Konzelmann & Fasel (1991) for early efforts (the DNS comparisons are reviewed by Reed 1994).

The Gaster & Grant (1975) work provided the foundation paper for looking at stability and transition phenomena that was not initiated by 2-D waves (and their subsequent interaction with

3-D) and as such, it is one of the important breakdown mechanisms that must be considered. It should be pointed out that one cannot rank the importance of different initial conditions that lead to transition because experience has shown that almost anything can happen.

Breuer & Haritonidis (1990) and Breuer & Landahl (1990) did linear experiments along with linear theory and temporal DNS for large disturbances in the case of an impulsive point disturbance. The linear results look classical although no direct comparison between theory and experiment is given. The nonlinear calculations, are useful in that they illustrate the presence of strongly inflected velocity profiles that could give rise to secondary instabilities.

5.2.5 Large-Amplitude-Disturbance Input

Under-resolved DNS solvers may possibly still capture the gross or mean features of transition. But this is not yet clear, and the present author suggests caution even if your goal is just a qualitative or ballpark prediction of transition location. If the details of the transition process are important, then this approach will more than likely give misleading results. Another observation with these high-freestream-turbulence computations is that there is definitely a need for accurate descriptions and cataloguing of the freestream environment, since transition has been well documented to be highly sensitive to this.

5.2.6 Supersonic/Hypersonic Flows

Following the discussion in Chapter 4, in contrast to incompressible flows, there is no guidance from experiments regarding the nonlinear stages of transition in supersonic and hypersonic flows. There is no comparable Klebanoff experiment. Initial CFD efforts have indicated that the amount of resources required can far exceed an incompressible calculation; gradients of disturbance quantities are generally steeper and compressibility is known to reduce disturbance amplitudes, thus "delaying" the normal appearance of breakdown in a given computational box. Supersonic and hypersonic flow are instances in which CFD (NPSE and DNS) must lead and guide what experiments should be performed and measurements taken for validation.

Thumm et al. (1990) and Bestek et al. (1992) studied spatially growing 3-D waves in a growing 2-D flat-plate boundary layer; the disturbances were introduced via periodic wall blowing/suction. They pointed out that a secondary instability calculation based on a finite 2-D amplitude may not be relevant for supersonic flow and they investigated other possible routes to turbulence at low supersonic Mach numbers. To this end they simulated a Mach-1.6 base flow subjected to a pair of 3-D waves and discovered a new breakdown mechanism, termed "oblique-wave breakdown". The disturbances quickly became nonlinear and through direct nonlinear interactions, a strong longitudinal vortex system was observed. The resulting structures, which differed from the Λ-shaped vortices usually reported for fundamental or subharmonic breakdown, were described as "honeycomb-like".

The inclusion of the bow shock is especially critical to studies of leading-edge receptivity and stability in hypersonics, as demonstrated by Zhong (1997). His DNS results over a blunt parabolic-leading-edge wedge at Mach 15 show that the instability waves developed behind the bow shock consist of both first and second modes. That is, free-stream acoustic disturbances can manifest themselves as first- and second-mode instabilities. The frequencies and growth rates found using DNS are comparable to those found using LST. His results also indicate that external disturbances, especially entropy and vorticity disturbances, enter the boundary layer to generate instability waves mainly in the leading-edge region. In an accompanying investigation, Hu and Zhong (1997) show a matching between a receptivity region and a linear growth region.

Furthermore, they show that disturbances found using the DNS approach have first-mode, second-mode, and shock-mode elements.

More recently, Zhong and Ma (2005) investigated receptivity mechanisms and instability mode interactions. They considered the receptivity of the blunted-cone flow investigated by Stetson et al. (1984), again showing a matching between a receptivity region and a linear-growth region. In a DNS simulation, all spatial and temporal scales of the flow are resolved by the simulation so that instability and transition mechanisms can be revealed by careful simulation and theoretical analysis of the results. DNS leads to large of amount of data which require analytical analysis in order to gain a deeper understanding of the underlining physics in hypersonic boundary-layer transition. A close collaboration between numerical and theoretical study will not only verify both sets of results, but also lead to better understanding of flow physics. Tumin et al. (2007) have been collaborating on joint theoretical and DNS studies of hypersonic boundary layer instability and receptivity mechanisms. As an example, direct numerical simulation of receptivity in a Mach 8 boundary layer over a sharp wedge of half-angle was carried out with perturbations introduced into the flow by blowing-suction through a slot. The perturbation flow-field downstream from the slot was decomposed into normal modes with the help of the biorthogonal eigenfunction system. Filtered-out amplitudes of two discrete normal modes and of the fast acoustic modes are compared with the linear receptivity problem solution. Figure 9 shows a comparison of the theoretical receptivity coefficient with the amplitude filtered out from the computational results by the theoretical analysis. One can see from the figure that there is an excellent agreement between amplitudes calculated with the help of the theoretical receptivity model.

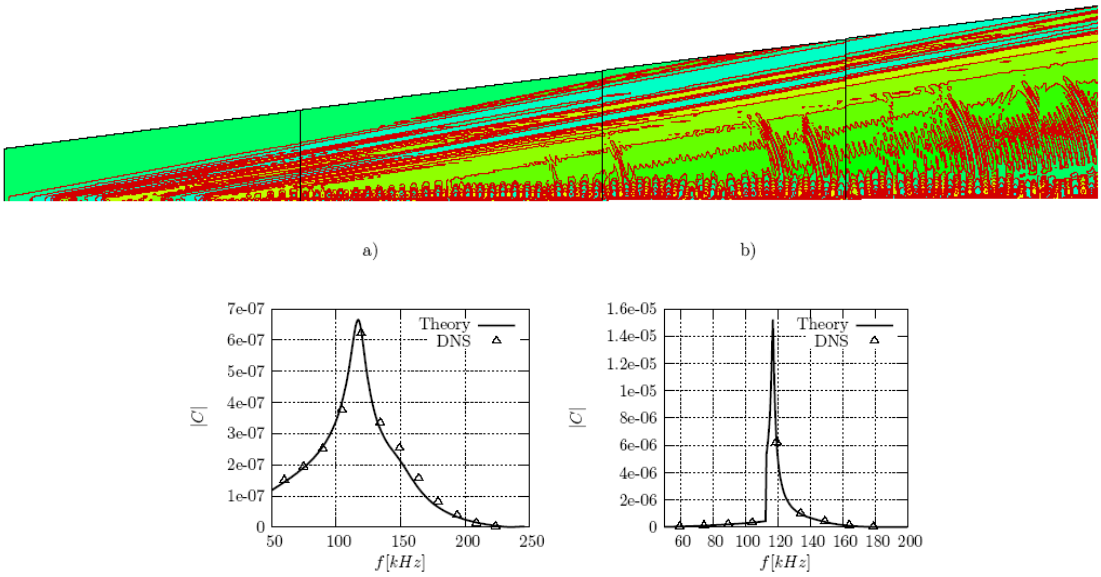

Figure 9. Numerical simulation of receptivity of the Mach 8 flow over a sharp wedge to wall blowing-suction: 1) instantaneous pressure perturbation field; 2) comparison of the theoretical prediction for the receptivity coefficient and comparison with data filtered out from the computational results (Tumin, Wang and Zhong 2007).

Much recent work has occurred investigating nonlinear breakdown mechanisms, including the 'classical' subharmonic breakdown scenario (Boutin et al., 2008 for a Mach 6 cone), and other new scenarios by Husmeier and Fasel (2007) for cones (both sharp and blunt cones) at Mach 8 under the Stetson wind-tunnel conditions (Stetson et al. 1983). In addition to oblique breakdown, Fasel identified several other nonlinear mechanisms that may cause transition. Typical results from these investigations are displayed in Figure 10, where the vortical structures over one spanwise wave length are shown (Figure 10, right). At the upstream end of the computational domain, close to the cone tip, the primary second-mode oblique waves dominate the flow structures, because the off-set between the structures over one streamwise wave length is equivalent to the wave angle of the primary wave (Ψ=20°). The spanwise extent of these structures decreases when the steady vortex (0,2) reaches high amplitude levels, as can be observed in Figure 10 (left). Far downstream, close to the outflow, all flow structures are aligned along two streaks associated with the longitudinal vortex (0,2). From these simulations, they have also found preliminary evidence how in the "noisy" Stetson experiments large nonlinear mechanisms are initiated by acoustic free stream disturbances, which excite large amplitude supersonic second mode disturbances and thus may lead directly to a bypass nonlinear breakdown

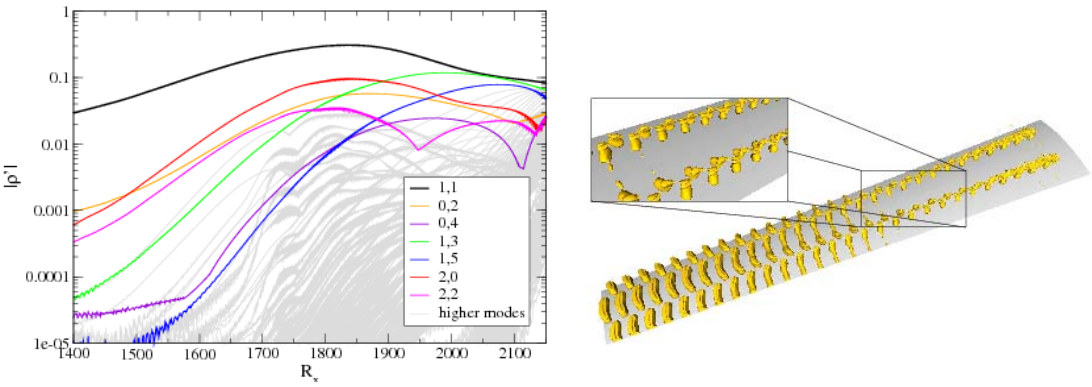

Figure 10. Oblique breakdown for the sharp cone at Mach 7.95 (Stetson wind tunnel conditions). Left: Streamwise ρ'-amplitude development. Right: Vortical structures. The nonlinear generation of higher modes (grey curves in the left figure) are an indication of the onset of the later stages of transition.

Fasel and his colleagues are also performing DNS in support of the ongoing and planned experiments in the M=3.5 quiet tunnel at NASA Langley Research Center. Towards this end, they have developed a new high-order accurate Navier-Stokes code, which is especially tailored towards accurate and efficient simulations of supersonic and hypersonic transition, in particular for cone geometries. This code has been thoroughly verified by comparing results obtained with small amplitude disturbances to LST (Laible et al. 2008). Preliminary nonlinear simulations for a circular cone at Mach 3.5 indicate that oblique breakdown may be a viable route to transition for the NASA wind tunnel conditions (see Figure 11). Moreover, the code has the capability of simulating effects of isolated 3D roughness elements.

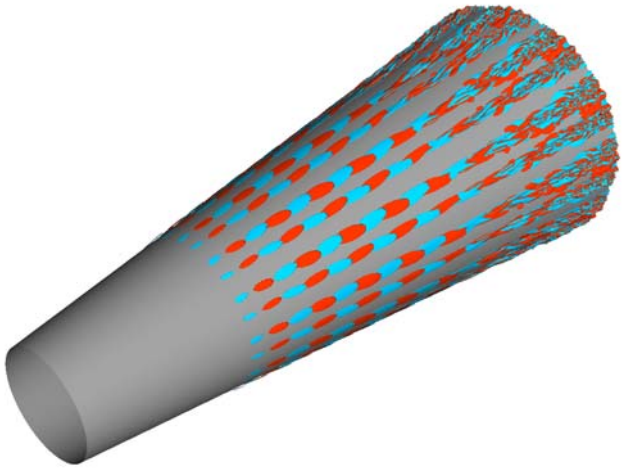

Figure 11. Oblique breakdown on 7°-cone at Mach 3.5 initiated by oblique wave with azimuthal mode number k_c = 12 and frequency F = 4.0 ·10^{-5}. Shown are isocontours of spanwise vorticity (blue: ω_x=-50, red: ω_x=50). NASA Langley M=3.5 quiet wind tunnel.

Most DNS studies of hypersonic boundary layer transition so far have been limited to "cold" hypersonic flow for which the perfect gas model can be used. For true hypersonic flight conditions, real gas effects, which include vibrational excitation, species dissociation/recombination, ionization, etc. are significant and have strong effects on the transition processes. Moreover, the effects of surface chemistry and ablation, the bow shock, nose bluntness, and the entropy layer are expected to be significant. Several groups are using DNS for simulating hypersonic flows with real effects, including Stemmer (2006) and X. Zhong's group at UCLA, and the community looks forward to understanding of the effects on transition. Also, DNS will aid in evaluating promising means of flow control, including ultrasonically absorptive coatings (UAC) that stabilize the second mode by extracting acoustic disturbance energy (Fedorov et al. 2001).

6.0 CONCLUDING REMARKS

DNS has been established as a viable framework and partner in the understanding of transition mechanisms. With the appropriate disturbance input conditions, the agreement among theory, computations, and experiments is remarkable, and from recent successes in the research community it is clear that advances in prediction methods and in identification of basic mechanisms will come from those groups working hand-in-hand:

- One must perform complementary computations and experiments on the same geometries and operating conditions.
- Because of sensitivity of transition to initial and operating conditions, computations provide validation of experiments and vice versa.

As we aspire to understand the effects of freestream disturbances and transition in high-speed, flight-Reynolds-number, and complex-geometry flows, this kind of collaboration becomes even

more critical. Detailed measurements are often more difficult and costly in these flows. Here, computations can guide the experiments as to what effects are important and what needs to be measured. As a good example, for flat-plate flow, computations have identified new breakdown mechanisms in high-speed flows different from those found in the seminal work of Klebanoff et al. (1962) and Herbert (1988) in low-speed flows, e.g. "oblique-wave breakdown" (Thumm et al., 1990).

REFERENCES

[1] Ackerberg, R., Phillips, J. 1972. The unsteady laminar boundary layer on a semi-infinite flat plate due to small fluctuations in the magnitude of the free-stream velocity. J. Fluid Mech. 51, 137-157.

[2] Arnal, D. 1994. Boundary layer transition: predictions based on linear theory, AGARD FDP/VKI Special Course on "Progress in Transition Modeling," AGARD Report No. 793, Madrid: 22-25 March 1993, Brussels: 29 March-1 April 1993.

[3] Bestek, H., Thumm, A., Fasel, H.F. 1992. Numerical investigation of later stages of transition in transonic boundary layers. First European Forum on Laminar Flow Technology, Hamburg, Germany, March.

[4] Bestek, H., Thumm, A., Fasel, H.F. 1992. Direct numerical simulation of the three-dimensional breakdown to turbulence in compressible boundary layers. Thirteenth International Conference on Numerical Methods in Fluid Dynamics, Rome, Italy, July.

[5] Boutin, D., Shiplyuk, A. Maslov, A., 2008, “Evolution of nonlinear processes in a hypersonic boundary layer on a sharp cone,” JFM, Vol. 611, pp.427-442.

[6] Breuer, K.S., Haritonidis, J.H. 1990. The evolution of a localized disturbance in a laminar boundary layer. Part 1. Weak disturbances. J. Fluid Mech., 220: 569.

[7] Breuer, K.S., Landahl, M.T. 1990. The evolution of a localized disturbance in a laminar boundary layer. Part 2. Strong disturbances. J. Fluid Mech. 220: 595.

[8] Buter, T.A., Reed, H.L. 1994. Boundary-layer receptivity to freestream vorticity. Phys. Fluids 6(10):3368-79

[9] Corke, T.C., Mangano, R.A. 1989. Resonant growth of three-dimensional modes in transitioning Blasius boundary layers, Journal of Fluid Mechanics 209, 93-150.

[10] Corke, T.C. 1990. Effect of controlled resonant interactions and mode detuning on turbulent transition in boundary layers. In Laminar-Turbulent Transition, ed. D. Arnal, R. Michel, pp. 151-78. Berlin: Springer-Verlag

[11] Corke, T.C. 1994. Digital time series processing for linear and nonlinear wave interactions in fluid instabilities. Transition: Experiments, Theory & Computations. Eds. T.C. Corke, G. Erlebacher, M.Y. Hussaini, Oxford.

[12] Craik, A.D.D. 1971. Nonlinear resonant instability in boundary layers. J. Fluid Mech. 50: 393.

[13] Erturk, E., Corke, T.C. 2001. Boundary layer leading edge receptivity to sound at incidence angles. J. Fluid Mech.

[14] Fasel, H.F. 1990. Numerical simulation of instability and transition in boundary layer flows, in Laminar-Turbulent Transition, (Arnal, D. and Michel, R., eds.), Springer-Verlag, Berlin.

[15] Fasel, H.F., Konzelmann, U. 1990. Nonparallel stability of a flat plate boundary layer using the complete Navier-Stokes equations, Journal of Fluid Mechanics 221, 311.

[16] Fasel, H.F., Rist, U., Konzelmann, U. 1987. Numerical investigation of the three-dimensional development in boundary layer transition, AIAA-87-1203.

[17] Fasel, H.F., Rist, U., Konzelmann, U. 1990. Numerical investigation of the three-dimensional development in boundary layer transition, AIAA Journal 28, 29.

[18] Fedorov, AV, Malmuth, ND, Rasheed, A, Hornung, HG (2001) AIAA Journal 39(4): 605-610.

[19] Fletcher, C.A.J. 1991. Computational Techniques for Fluid Dynamics, Volumes I & II, Springer Series in Computational Physics, (Glowinski, R. et al., eds.), Springer-Verlag, New York.

[20] Fuciarelli DA, Reed HL, Lyttle I. 2000. Direct numerical simulation of leading-edge receptivity to sound. AIAA J. 38(7):1159-65

[21] Gaster, M., Grant, I. 1975. An experimental investigation of the formation and development of a wave packet in a laminar boundary layer, Proceedings of the Royal Society of London A347, 253.

[22] Goldstein, M.E. 1983. The evolution of Tollmien-Schlichting waves near a leading edge, Journal of Fluid Mechanics 127, 59-81.

[23] Goldstein, M.E. 1985. Scattering of acoustic waves into Tollmien-Schlichting waves by small streamwise variations in surface geometry, Journal of Fluid Mechanics 154, 509-530.

[24] Goldstein, M.E., Hultgren, L.S. 1987. A note on the generation of Tollmien-Schlichting waves by sudden surface-curvature change, Journal of Fluid Mechanics 181, 519-525.

[25] Goldstein, M., Hultgren, L. 1989. Boundary-layer receptivity to long-wave freestream disturbances. Ann. Rev. Fluid Mech. 21, 137-166.

[26] Goldstein, M., Sockol, P., Santz, J. 1983. The evolution of Tollmien-Schlicting waves near a leading edge. Part 2. Numerical determination of amplitudes. J. Fluid Mech. 129, 443-453.

[27] Gresho, P.M. 1991. Incompressible fluid dynamics: some fundamental formulation issues, Annual Review of Fluid Mechanics 23, 413-453.

[28] Gresho, P.M., Sani, R.L. 1987. On pressure boundary conditions for the incompressible Navier-Stokes equations, International Journal of Numerical Methods in Fluids 7, 1111-1145.

[29] Haddad, O., Corke, T. 1998. Boundary layer receptivity to freestream sound on parabolic bodies. J. Fluid Mech.

[30] Hammerton, P., Kerschen, E. 1996. Boundary-layer receptivity for a parabolic leading edge. J. Fluid Mech. 310, 243-267.

[31] Hammerton, P., Kerschen, E. 1997. Boundary-layer receptivity for a parabolic leading edge. Part 2. The small Strouhal number limit. J. Fluid Mech. 353, 205-220.

[32] Hammerton, P.W., Kerschen, E.J. 2000. Effect of leading –edge geometry and aerodynamic loading on receptivity to acoustic disturbances, in Laminar-Turbulent Transition, (Fasel, H. and Saric, W., eds.), Springer-Verlag, pp. 37-42

[33] Heinrich, R., Choudhari, M., Kerschen, E. 1988. A comparison of boundary-layer receptivity mechanisms. AIAA Paper 88-3758.

[34] Heinrich, R., Kerschen, E. 1989. Leading-edge boundary layer receptivity to various free-stream disturbance structures. Z.Angew.Math.Mech.69, T596-598.

[35] Herbert, T. 1984. Secondary instability of shear flows. Special Course on Stability and Transition of Laminar Flows, AGARD Report No. 709, March 1984

[36] Herbert, Th. 1988. Secondary instability of boundary layers, Annual Review of Fluid Mechanics 20, 487-526.

[37] Husmeier, F., Fasel, H.F., 2007. “Numerical Investigations of Hypersonic Boundary Layer Transition for Circular Cones,” AIAA-2007-3843.

[38] Joslin, R.D., Streett, C.L. 1992. A preliminary study of crossflow transition on a swept wing by spatial direct numerical simulation, Instability, Transition, and Turbulence, (Hussaini, M.Y., Kumar, A., and Streett, C.L., eds.), Springer-Verlag, New York.

[39] Joslin, R.D., Streett, C.L. 1992. Crossflow disturbance evolution on swept wings computed by spatial DNS, Bulletin of the American Physical Society 37, 8, 1778.

[40] Joslin, R.D., Streett, C.L., Chang, C.-L. 1992. Validation of three-dimensional incompressible spatial direct numerical simulation code: a comparison with linear stability and parabolic stability equation theories for boundary-layer transition on a flat plate, NASA Technical Paper 3205.

[41] Joslin, R.D., Streett, C.L., Chang, C.-L. 1992. Spatial direct numerical simulation of boundary-layer transition mechanisms: validation of PSE theory. Theoretical and Computational Fluid Dynamics.

[42] Kachanov, Yu.S., Kozlov, V.V., Levchenko, V.Ya. 1977. Nonlinear development of a wave in a boundary layer (in Russian). Mekhanika Zhidkosti i Gaza 3: 49

[43] Kachanov, Yu.S., Levchenko, V.Ya. 1984. The resonant interaction of disturbances at laminar-turbulent transition in a boundary layer, Journal of Fluid Mechanics 138, 209-247.

[44] Kendall, J.M. 1984. Experiments on the generation of Tollmien-Schlichting waves in a flat plate boundary layer by weak freestream turbulence. AIAA Pap. No. 84-0011

[45] Kendall, J.M. 1991. Studies on laminar boundary-layer receptivity to freestream turbulence near a leading edge, FED-Vol. 114, Boundary Layer Stability and Transition to Turbulence, (Reda, D.C., Reed, H.L., and Kobayashi, R., eds.), ASME.

[46] Kendall, J.M. 1998. Experiments on boundary-layer receptivity to freestream turbulence. AIAA Pap. No. 98-0530

[47] Kerschen, E.J. 1989. Boundary layer receptivity, AIAA-89-1109.

[48] Kerschen, E.J., Choudhari, M., Heinrich, R.A. 1990. Generation of boundary instability waves by acoustic and vortical freestream disturbances, in Laminar-Turbulent Transition, (Arnal, D. and Michel, R., eds.), Springer-Verlag, Berlin, pp. 477-88

[49] Klebanoff, P.S., Tidstrom, K.D., Sargent, L.M. 1962. The three-dimensional nature of boundary-layer instability, Journal of Fluid Mechanics 12, 1-34.

[50] Kleiser, L., Zang, T.A. 1991. Numerical simulation of transition in wall-bounded shear flows, Annual Review of Fluid Mechanics 23, 495-537.

[51] Kobayashi, R. ed. 1995. Laminar-Turbulent Transition IV. Berlin: Springer. 532 pp.

[52] Konzelmann, U., Fasel, H.F. 1991. Numerical simulation of a three-dimensional wave packet in a growing flat plate boundary layer, Boundary Layer Transition and Control Conference, 8-12 April, Peterhouse College, Cambridge, U.K.

[53] Kosorygin, V.S., Radeztsky, R.H. Jr., Saric, W.S. 1995. Laminar boundary layer sound receptivity and control, in Laminar-Turbulent Transition, (Kobayashi, ed.), Springer-Verlag, pp. 517-24

[54] Kozlov, V.V., Ramazanov, M.P. 1984. Development of finite amplitude disturbances in a Poiseuille flow. J. Fluid Mech. 147: 149

[55] Kral, L.D., Fasel, H.F. 1989. Numerical investigation of the control of the secondary instability process in boundary layers, AIAA-89-0984.

[56] Kral, L.D., Fasel, H.F. 1990. Numerical simulation of the control of the three-dimensional transition process in boundary layers, in Laminar-Turbulent Transition, (Arnal, D. and Michel, R., eds.), Springer-Verlag, Berlin.

[57] Laible, A., Mayer, C., Fasel, H., 2008, “Numerical Investigation of Supersonic Transition for a Circular Cone at Mach 3.5,” AIAA-2008-4397.

[58] Lam, S., Rott, N. 1960. Theory of linearized time-dependent boundary layers. Cornell Univ. Grad. School of Aero. Engineering Rep. AFOSR TN-60-1100.

[59] Lam, S., Rott, N. 1993. Eigen-functions of linearized unsteady boundary layer equations. ASME I: J. Fluids Engrg 115, 597-602.

[60] Lin, N., Reed, H.L., Saric, W.S. 1992. Effect of leading-edge geometry on boundary-layer receptivity to freestream sound, Instability, Transition, and Turbulence, (Hussaini, M.Y., Kumar, A., and Streett, C.L., eds.), Springer-Verlag, New York.

[61] Mack, L.M. 1984. Line sources of instability waves in a Blasius boundary layer. AIAA Pap. No. 84-0168

[62] Mack, L.M. 1984. Boundary-layer linear stability theory. AGARD Rep. No. 709 (Special course on stability and transition of laminar flows), Von Kármán Inst., Rhode-St.-Genese, Belg.

[63] Malik, M.R. 1990. Numerical methods for hypersonic boundary layer stability. J. Comp. Physics 86: 376-413

[64] Malik, M.R. 1990. Stability theory for chemically reacting flows. In Laminar-Turbulent Transition, ed. D. Arnal, R. Michel, pp. 251-60. Berlin: Springer-Verlag

[65] Nishioka, M., Iida, S., Ichikawa, Y. 1975. An experimental investigation of the stability of plane Poiseuille flow, J. Fluid Mech. 72: 731

[66] Nishioka, M., Asai, M., Iida, S. 1980. An experimental investigation of secondary instability. Laminar-Turbulent Transition, Vol. I., eds: R. Eppler, H. Fasel, Springer

[67] Oberkampf, W.L., Blottner, F.G., Aeschliman, D.P. 1995. Methodology for computational fluid dynamics code verification/validation. AIAA Paper 95-2226.

[68] Parekh, D.E., Pulvin, P., Wlezien, R.W. 1991. Boundary layer receptivity to convected gusts and sound, FED-Vol. 114, Boundary Layer Stability and Transition to Turbulence, (Reda, D.C., Reed, H.L., and Kobayashi, R., eds.), ASME.

[69] Reed, H.L. 1994. Direct numerical simulation of transition: The spatial approach. AGARD Rep. No. 793 (Special course on progress in transition modelling), Von Kármán Inst., Rhode-St.-Genese, Belg.

[70] Rist, U., Kachanov, V. 1995. Numerical and experimental investigation of the K-regime of boundary-layer transition. In Laminar-Turbulent Transition, ed. R. Kobayashi, pp. 405-412. Berlin: Springer-Verlag

[71] Roache, P.J. 1985. Computational Fluid Mechanics, Hermosa Publishers, Albuquerque.

[72] Roache, P. 1997. Quantification of uncertainty in computational fluid dynamics. Annual Review of Fluid Mechanics, Vol. 29, pp. 123-160.

[73] Saric, W.S., Kozlov, V.V., Levchenko, V.Ya. 1984. Forced and unforced subharmonic resonance in boundary-layer transition. AIAA Paper No. 84-0007

[74] Saric, W.S. 1986. Visualization of different transition mechanisms. Physics of Fluids, Vol.29, pp. 2770.

[75] Saric, W.S. 1994. Physical description of boundary-layer transition: experimental evidence, AGARD FDP/VKI Special Course on "Progress in Transition Modeling," AGARD Report No. 793, Madrid: 22-25 March 1993, Brussels: 29 March-1 April 1993.

[76] Saric, W.S. 1994. Görtler vortices, Annual Review of Fluid Mechanics 26, 379-409.

[77] Saric, W., Reed, H., Kerschen, E. 1994. Leading-edge receptivity to sound: experiments, DNS, theory. Invited Paper, AIAA-94-2222, Colorado Springs.

[78] Saric, W.S., Thomas, A.S.W. 1984. Experiments on the subharmonic route to turbulence in boundary layers. In Turbulence and Chaotic Phenomena in Fluids, ed. T. Tatsumi. Amsterdam: North-Holland

[79] Saric, W., White, E. 1998. Influence of high-amplitude noise on boundary-layer transition to turbulence. AIAA-98-2645.

[80] Saric, W.S., Reed, H.L., White, E.B. 1999. Boundary-layer receptivity to freestream disturbances and its role in transition. AIAA Pap. No. 99-3788

[81] Saric, W., Reed, H., Kerschen, E. 2002. Boundary-layer receptivity. Annual Review of Fluid Mechanics 34, 291-319.

[82] Singer, B.A., Reed, H.L., Ferziger, J.H. 1986. Investigation of the effects of initial disturbances on plane channel transition. AIAA Paper No. 86-0433

[83] Singer, B.A., Reed, H.L., Ferziger, J.H. 1989. The effect of streamwise vortices on transition in the plane channel, Physics of Fluids A 1, 12, 1960.

[84] Spalart, P.R. 1984. Numerical simulation of boundary-layer transition. NASA-TM-85984

[85] Spalart, P.R., Yang, K.S. 1987. Numerical study of ribbon-induced transition in Blasius flow. J. Fluid Mech. 178, 345

[86] Spalart, P.R. 1989. Direct numerical study of leading-edge contamination, AGARD-CP-438.

[87] Spalart, P.R. 1990. Direct numerical study of crossflow instability, in Laminar-Turbulent Transition, (Arnal, D. and Michel, R., eds.), Springer-Verlag, Berlin.

[88] Spalart, P.R. 1991. On the crossflow instability near a rotating disk, Boundary Layer Transition and Control Conference, 8-12 April, Peterhouse College, Cambridge, U.K.

[89] Spalart, P.R. 1993. Numerical study of transition induced by suction devices, Proceedings of the International Conference on Near Wall Turbulent Flows (So, R.M.C., ed.), March 15-17, Elsevier.

[90] Steinberg, S., Roache, P. 1985. Symbolic manipulation and computational fluid dynamics. Journal of Computational Physics, Vol. 57, pp. 251-284.

[91] Stemmer, C. 2006. Transition investigation on hypersonic flat-plate boundary layers flows with chemical and thermal non-equilibrium. IUTAM Symposium on Laminar-Turbulent Transition, R. Govindarajan (ed.), Springer, 363–368.

[92] Stetson, K. F., Thompson, E. R., Donaldson, J. C., Siler, L. G., 1983, "Laminar Boundary Layer Stability Experiments on a Cone at Mach 8; Part I: Sharp Cone," AIAA-Paper 83-1761.

[93] Stetson, K.F., Thompson, E.R., Donaldson, J.C., Siler L.G. 1984. Laminar boundary layer stability experiments on a cone at Mach 8, part 2: blunt cone. AIAA 84-0006.

[94] Streett, C.L., Macaraeg, M.G. 1989. Spectral multi-domain for large scale fluid dynamic simulations, Applied Numerical Mathematics 6, 1, 23.

[95] Tani, I. 1981. Three-dimensional aspects of boundary-layer transition. Proc. Indian Acad, Sci. 4: 219

[96] Thomas, A.S.W., Saric, W.S. 1981. Harmonic and subharmonic waves during boundary-layer transition. Bull. Amer. Phys. Soc. 26: 1252

[97] Thompson, K.W. 1987. Time dependent boundary conditions for hyperbolic systems, Journal of Computational Physics 68, 1-24.

[98] Thumm, A., Wolz, W., Fasel, H.F. 1990. Numerical simulation of spatially growing three-dimensional disturbance waves in compressible boundary layers, in Laminar-Turbulent Transition, (Arnal, D. and Michel, R., eds.), Springer-Verlag, Berlin.

[99] Tumin, A., Wang, X., Zhong, X., 2007, "Direct numerical simulation and the theory of receptivity in a hypersonic boundary layer," Physics of Fluids, 19, 014101 (1-14).

[100] Wanderly, J.B.V., Corke, T.C. 2001. Boundary layer receptivity to free-steam sound on elliptic leading edges of flat plates. J. Fluid Mech. 429:1-29

[101] Zhong, X. 1997. Direct numerical simulation of hypersonic boundary-layer transition over blunt leading edges, part II: receptivity to sound. Paper 97-0756, AIAA, January.

[102] Zhong, X., and Ma, Y., 2005, "Boundary-layer receptivity of Mach 7.99 Flow over a blunt cone to free-stream acoustic waves," Journal of Fluid Mechanics, 556: p. 55-103.